

SACLANTCEN REPORT
serial no.: SR-235

**SACLANT UNDERSEA
RESEARCH CENTRE**

REPORT



**Detection of buried mines
using Rayleigh-scattered
second-derivative Gaussian pulses**

P.H. Rogers

October 1995

The SACLANT Undersea Research Centre provides the Supreme Allied Commander Atlantic (SACLANT) with scientific and technical assistance under the terms of its NATO charter, which entered into force on 1 February 1963. Without prejudice to this main task – and under the policy direction of SACLANT – the Centre also renders scientific and technical assistance to the individual NATO nations.

This document is released to a NATO Government at the direction of SACLANT Undersea Research Centre subject to the following conditions:

- The recipient NATO Government agrees to use its best endeavours to ensure that the information herein disclosed, whether or not it bears a security classification, is not dealt with in any manner (a) contrary to the intent of the provisions of the Charter of the Centre, or (b) prejudicial to the rights of the owner thereof to obtain patent, copyright, or other like statutory protection therefor.
- If the technical information was originally released to the Centre by a NATO Government subject to restrictions clearly marked on this document the recipient NATO Government agrees to use its best endeavours to abide by the terms of the restrictions so imposed by the releasing Government.

Page count for SR-235
(excluding Covers
and Data Sheet)

Pages	Total
i-vi	6
1-44	44
	<hr/> 50

SACLANT Undersea Research Centre
Viale San Bartolomeo 400
19138 San Bartolomeo (SP), Italy

tel: +39-187-540.111
fax: +39-187-524.600

e-mail: library@saclantc.nato.int

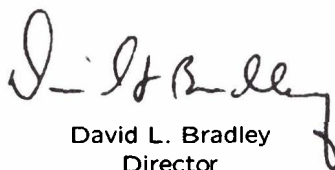
NORTH ATLANTIC TREATY ORGANIZATION

SACLANTCEN SR-235

Detection of buried mines
using Rayleigh-scattered
second-derivative Gaussian pulses

P.H. Rogers

The content of this document pertains
to work performed under Project 25 of
the SACLANTCEN Programme of Work.
The document has been approved for
release by The Director, SACLANTCEN.



David L. Bradley
Director

SACLANTCEN SR-235

SACLANTCEN SR-235

**Detection of buried mines using
Rayleigh-scattered second-derivative
Gaussian pulses**

P.H. Rogers

Executive Summary: The enclosed report is a theoretical study to determine if it is feasible to use low frequencies (< 1000 Hz) for detection of buried mines in the seafloor. In-stride detection and classification of sea mines will only be possible with large areal coverage and that, in turn requires either complex high-frequency systems or lower-frequency techniques with larger transmission ranges and better seafloor penetration capability. This study investigates a novel method of exploiting the differences in density and mechanical properties (mainly bulk modulus) between the seafloor and the buried mine. The results of the study are promising in that calculations for a wide range of sediment types and reasonable mine properties indicate sufficient echo strength is present to allow detection. It (the study) is promising enough that an experiment is planned for either late 1995 or early 1996.

SACLANTCEN SR-235

SACLANTCEN SR-235

**Detection of buried mines using
Rayleigh-scattered second-derivative
Gaussian pulses**

P.H. Rogers

Abstract: Large ground mines which are intentionally or unintentionally buried in the sediment have proven to be difficult to detect. This report is the result of a study undertaken by the author while on leave from Georgia Tech at the NATO SACLANT Undersea Research Centre. It considers the possibility that low-frequency (200–500 Hz) pulses could be used to detect and localize buried mines. It has been shown that it may be possible to detect buried mines using Rayleigh scattered second derivative Gaussian pulses. The robustness of the method stems from the differences in mechanical properties of the mine and the wide range of bulk modulus and density of seafloor sediments.

Keywords: buried mines ◦ detection ◦ Gaussian pulse ◦ low frequency ◦ Rayleigh scattering

Contents

1. System configuration and rationale	1
2. Rayleigh scattering from a buried mine	4
3. Transmitted pulse and target echoes	13
4. Reverberation	19
5. Detectability of buried mines	34
6. Conclusions and recommendations	41
References	42

1

System configuration and rationale

The approach is to exploit the fairly robust Rayleigh echo in the 200–500 Hz frequency range where ka is sufficiently small for Rayleigh scattering to be appropriate but still large enough to produce a sizable echo ($ka \approx 0.2$ – 0.5). In the Rayleigh regime there will be an echo as long as the compliance or density of the mine differs from that of the sediment in which it is buried. The robustness stems from the rather wide range in the bulk modulus and density of water and the various sediments found in shallow water (see Table 1.1). The densities range over a factor of 2 and the moduli over a factor of 2.5. The likelihood of a mine matching both the density and compliance of the sediment in which it happens to be buried, is small. In addition, as will be shown in Sect. 2, the effective Rayleigh target strength of a mine usually increases when it is buried.

Table 1.1 Typical sediment parameters for the continental terrace (from Hamilton, 1980)

Sediment Type	Density (kg/m^3)	Porosity (%)	Sound Speed Ratio	Attenuation (dB/λ_A)	Bulk Modulus (GPa)
Fine Sand	1941	45.6	1.145	0.75	5.726
Sandy Silt	1771	54.1	1.08	1.03	4.65
Silt	1740	56.3	1.057	0.9	4.374
Sand Silt Clay	1596	66.3	1.033	0.18	3.832
Clayey Silt	1488	71.6	1.014	0.15	3.442
Silty Clay	1421	75.9	0.994	0.14	3.159
Water	1000	-	1.000	$\sim .0002$	2.250

The source/receiver is located fairly close to the bottom. Throughout this report we will assume, for concreteness, that it is located $z = 5$ m off the bottom. The source/receiver could be towed by a mine countermeasures (MCM) ship but is small enough to be deployed from an unmanned underwater vehicle (UUV). The UUV would be the preferred platform. The omnidirectional source radiates a relatively short, high-amplitude, broadband, low-frequency (200–500 Hz) pulse. The pulse is a second-derivative Gaussian. (See Sect. 3 for a discussion and description of the pulse and its generation.) The pulse has a total length τ_L of about 5 msec but the length of the reflected pulse between the 3 dB down points, τ is less than 0.5 msec.

The geometry for a water depth $d_w = 30$ is illustrated in Fig. 1.1. If the pulse is launched at time $t=0$, the reflection from the bottom will begin to be detected at the receiver at $t = 2z/c$ and will have completely passed the receiver by $t=2z/c + \tau_L$. Detections will not be possible, due to contamination by the bottom reflection (and the direct signal), for lateral ranges less than

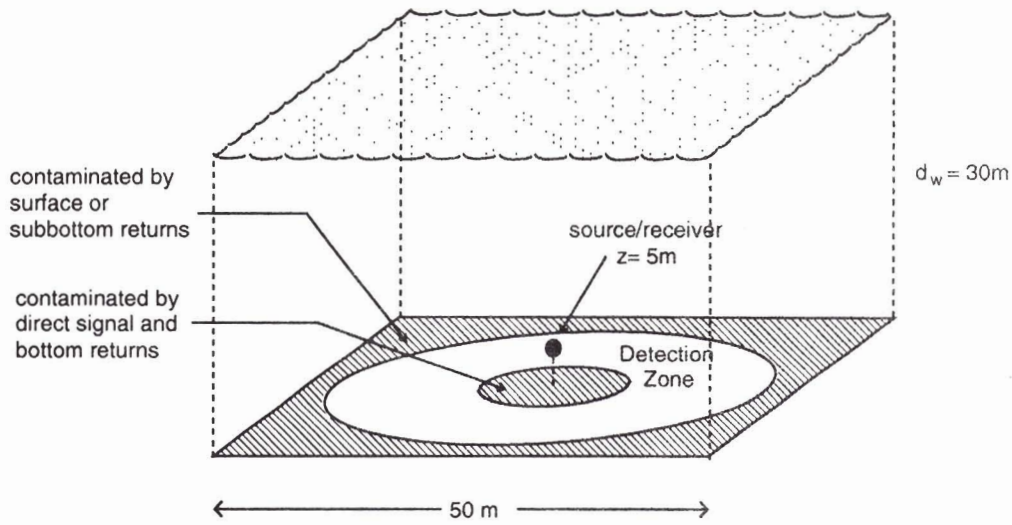


Figure 1.1 Geometry of the problem approximately to scale for a water depth of 30 m. Shaded areas are regions where detection is not possible.

$$w_{\min} = \sqrt{\left(z + \frac{c\tau_L}{2}\right)^2 - z^2} \quad (1.1)$$

where c is the speed of sound in water. For our case ($z = 5$ and $\tau_L = 5$ msec) w_{\min} is 7 m. If the signal-to-noise and signal-to-reverberation ratios are sufficiently large, a buried target can be detected from this range, outward, until surface (or subbottom) reflections begin to arrive at the sensor. This will occur when $t = 2(d_w - z)/c$. The corresponding maximum detection range is given by

$$w_{\max} = \sqrt{(d_w - z)^2 - z^2} \quad (1.2)$$

If the subbottom reflection is the limiting interference, the negative of the sediment thickness replaces water depth in Eq. (1.2). For the example shown in Fig. 1.1, $d_w = 30$ so $w_{\max} = 25$ m. The *detection zone* (see Fig. 1.1) is a ring of inner radius w_{\min} and outer radius w_{\max} . With a rate of advance of 4 m/s the search rate would be 200 m²/sec. However, if the ambient noise is high, a detection range equal to w_{\max} may only be achievable (with a single sensor) by averaging over several pulses (see Sect. 5). In this case (depending on the allowable pulse repetition rate) a 4 m/s rate of advance may be too fast. Narrowing the swath and maintaining or increasing the rate of advance may be preferable.

The range resolution is given by

$$\Delta w \approx \tau c / 2 \quad (1.3)$$

which for our parameters is less than 40 cm. This is smaller than the size of a typical ground mine. (A typical ground mine is a cylinder, around 2.5 m long and 0.5 m in diameter.) A single detection localize the mine to a ring of thickness Δw . Two detections along a straight line track localize the mine to either of two regions (which are of the order of the size of the mine) on either side of the track. Multiple detections along a non-straight-line track unambiguously localize the mine.

It would be desirable to measure horizontal acoustic particle motion in addition to pressure. This could be done using neutrally buoyant displacement sensors (or accelerometers). In high signal-to-reverberation situations particle motion detectors would enable the simultaneous determination of bearing along with range (using an arctangent algorithm). In low signal-to-reverberation situations they would, at least, resolve the left-right ambiguity. Such sensors would also help to discriminate between mine echoes and reflections from subbottom layers since they would not respond to the latter if the layers are nearly horizontal.

Cylindrical mines have echoes which are aspect dependent, being largest at broadside (see Sect. 3 for details). As the sonar passes the mine, however, at some point it must be broadside (or nearly broadside) to it. Thus the only case where poor target orientation could prevent detection is if the mine is on, or close to, the source track and is oriented parallel to it. In this case the mine would have to be detected on a subsequent (or prior) search leg.

The remainder of this report investigates the question of whether signal-to-reverberation and signal-to-noise levels would allow such a scheme to work.

2

Rayleigh scattering from a buried mine

Acoustic scattering from nonresonant objects which are much smaller than an acoustic wavelength is referred to as Rayleigh scattering. It is characterized by a scattered pressure which is proportional to frequency squared for sinusoidal incident pressure or, equivalently, for an arbitrary pressure time waveform, to the second derivative of the incident pressure, $\partial^2 p / \partial t^2$. Rayleigh scattering consists of two terms, an omnidirectional term which is due to volume changes in the scattering object induced by the incident pressure, and a dipole term which is due to pressure-gradient-induced oscillation of the scattering object. The omnidirectional term will be present whenever the volume compliance of the object differs from that of the surrounding fluid, and the dipole term will be present whenever the density of the object differs from the density of the surrounding fluid. We will consider primarily the compliance-related omnidirectional term which is expected to be larger and more robust than the density-related dipole term for the buried mine problem. The density of a ground mine is typically much greater than that of water but when buried may have very nearly the same density as the sediment. The effect of Rayleigh scattering due to density difference will be included as an approximate correction term. (The expected compliance of a ground mine is discussed in Sect. 3.) The geometry of the problem is illustrated in Fig. 2.2.

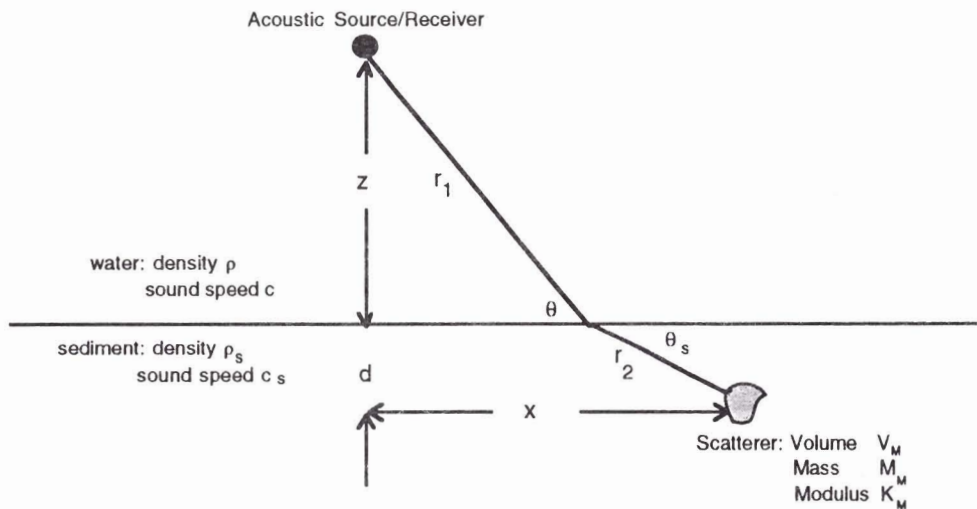


Figure 2.1 *Geometry of the problem (object buried in sediment)*

The sound source and receiver are located at a distance z above the sea floor. The scattering object is buried at a depth d beneath the sea floor and at a horizontal distance x from the source. Its volume is V_m , its mass is M_m and its effective bulk modulus is K_m . The speed of sound in the water is c and its density is ρ . The sediment is considered to be a fluid with sound (complex) speed c_s and density ρ_s .

The sound pressure in the water at a distance r from a simple source with volume acceleration $\ddot{V}(t)$ is given by

$$p_w(r, t) = \frac{\rho}{4\pi r} \ddot{V}(t - r/c) \quad (2.1)$$

Assuming, sinusoidal excitation with $\ddot{V}(t) = -\omega^2 \hat{V}_0 e^{-i\omega t}$, Eq. (2.1) becomes

$$p_w(r, \theta, t) = -\omega^2 \frac{\rho \hat{V}_0}{4\pi r} e^{i(kr - \omega t)} = \hat{p}_0 \frac{r_0}{r} e^{i(kr - \omega t)} \quad (2.2)$$

where $\hat{p}_0 r_0$ is the sound pressure at the reference range, $r_0 (= 1 \text{ m})$, and $k = \omega/c$ is the wave number.

From energy considerations, it can be shown that for grazing angles greater than the critical angle ($\theta > \theta_c = \cos^{-1}(c/c_s)$), if the pressure in the water is given by Eq. (2.2), the pressure in the sediment at the location of the buried object is given by

$$\hat{p}_{inc}(r_m, \theta, t) = -\omega^2 \frac{\rho \hat{V}_0}{4\pi} T(\theta) \left(\frac{\frac{c}{\sin \theta}}{\frac{cr_1}{\sin \theta} + \frac{c_s r_2}{\sin \theta_s}} \right) e^{i(kr_1 + k_s r_2 - \omega t)} \quad (2.3)$$

where $r_m = \sqrt{(z+d)^2 + x^2}$ is the distance from source to the buried object and $\hat{T}(\theta)$ is the plane wave transmission coefficient from water to sediment given by

$$\hat{T}(\theta) = \frac{\frac{2\rho_s c_s}{\Gamma_s}}{\frac{\rho_s c_s}{\Gamma_s} + \frac{\rho c}{\sin \theta}} \quad (2.4)$$

where

$$\begin{aligned} \Gamma_s &= \sqrt{1 - \frac{c_s^2}{c^2} \cos^2 \theta} \\ &= \sin \theta_s \quad \text{for } \theta > \theta_c \end{aligned} \quad (2.5)$$

In general, T is complex because c_s is complex.

If $d \ll z$, and $c \approx c_s$, Eq. (2.4) can be simplified so that the incident pressure in the sediment is

$$\hat{p}_{inc}(r_m, \theta, t) = -\omega^2 \frac{\rho \hat{V}_0}{4\pi r_m} \hat{T}(\theta) e^{i(kr_m - \omega t)} = \hat{p}_0 \frac{r_0}{r_m} \hat{T}(\theta) e^{i(kr_m - \omega t)} \quad \text{for } \theta > \theta_c \quad (2.6a)$$

For critical reflection, $\theta < \theta_c$, Γ_s becomes imaginary and the field in the sediment becomes evanescent. The incident pressure in Eq. (2.6a) must then be modified to correct for the exponential decay in the sediment

$$\hat{p}_{inc}(r, \theta, t) = \hat{p}_0 \frac{r_0}{r_m} \hat{T}(\theta) e^{-|\Gamma_s| k_s d} e^{i(k r_m - \omega t)} \quad \text{for } \theta < \theta_c \quad (2.6b)$$

where $k_s = \omega/c_s$.

The incident pressure induces a volume change in the scattering object given by

$$\delta V_m = \left(\frac{1}{K_m} \right) V_m \hat{p}_{inc}(r_m, \theta, t) \quad (2.7)$$

where K_m is the effective bulk modulus of the object. The corresponding volume change that would be induced in the displaced sediment is given by

$$\delta V_s = \left(\frac{1}{\rho_s c_s^2} \right) V_m p_{inc}(r_m, \theta, t) \quad (2.8)$$

The scattered field can be obtained by solving the radiation problem for a source with a volume change given by the difference between Eq. (2.7) and Eq. (2.8)

$$\delta V_{scat} = \delta V_m - \delta V_s = \left(\frac{1}{K_m} - \frac{1}{\rho_s c_s^2} \right) V_m p_{inc}(r_m, \theta, t) \quad (2.9)$$

Thus from Eq. (2.1) and Eq. (2.9), within the sediment, at a distance r' from the scatterer the scattered pressure would be

$$\hat{p}_{scat}(r') = -\frac{\rho_s}{4\pi r'} \omega^2 \delta V_{scat} = -\frac{\rho_s}{4\pi r'} \omega^2 V_m \frac{\beta_m}{\rho_s c_s^2} p_{inc}(r_m, \theta, t) \quad (2.10)$$

where the monopole coefficient β_m is defined by

$$\beta_m = \frac{1 - K_m / \rho_s c_s^2}{K_m / \rho_s c_s^2} \quad (2.11)$$

The backscattered pressure (within the water) at the source can be obtained from reciprocity. Reciprocity requires that the pressure at the source due to a given volume acceleration of the scatterer must be equal to the pressure at the scatterer due to an equal volume acceleration of the source. The pressure at the scatterer which would result from a volume acceleration of the source of $-\omega^2 \delta V_{scat}$ is given by Eq. (2.6a) and Eq. (2.6b) with \hat{V}_0 replaced by $\delta V_{scat} / 4\pi$. Hence the backscattered pressure is given by

$$\begin{aligned} \hat{p}_{scat} &= -\frac{\rho}{4\pi} \omega^2 \hat{T}(\theta) \frac{1}{r_m} V_m \frac{\beta_m}{\rho_s c_s^2} p_{inc}(r_m, \theta, t - r_m / c) & \text{for } \theta < \theta_c \\ \hat{p}_{scat} &= -\frac{\rho}{4\pi} \omega^2 \hat{T}(\theta) \frac{1}{r_m} e^{-|\Gamma_s| k_s d} V_m \frac{\beta_m}{\rho_s c_s^2} p_{inc}(r_m, \theta, t - r_m / c) & \text{for } \theta > \theta_c \end{aligned} \quad (2.12)$$

Finally, substituting Eq. (2.6a) and Eq. (2.6b) for p_{inc} in Eq. (2.12) we get

$$\begin{aligned}\hat{p}_{scat} &= -\frac{\rho}{4\pi} \omega^2 \left(\hat{T}(\theta) \right)^2 \frac{\hat{p}_0 r_0}{r_m^2} V_m \frac{\beta_m}{\rho_s c_s^2} e^{i(2kr_m - \omega t)} & \text{for } \theta < \theta_c \\ \hat{p}_{scat} &= -\frac{\rho}{4\pi} \omega^2 \left(\hat{T}(\theta) \right)^2 \frac{\hat{p}_0 r_0}{r_m^2} e^{-2|\Gamma_s|k_s d} V_m \frac{\beta_m}{\rho_s c_s^2} e^{i(2kr_m - \omega t)} & \text{for } \theta < \theta_c\end{aligned}\quad (2.13)$$

If the same object were not buried in the sediment but instead was freely suspended in the water at the same distance from the source/receiver the scattered pressure would be given by

$$(\hat{p}_{scat})_{\text{not buried}} = -\frac{\rho}{4\pi} \omega^2 \frac{\hat{p}_0 r_0}{r_m^2} V_m \left(\frac{1}{K_m} - \frac{1}{\rho c^2} \right) e^{i(2kr_m - \omega t)} \quad (2.14)$$

Thus burying the mine has the effect of increasing its TS by a factor of

$$\Delta TS = 20 \log_{10} \left(T(\theta)^2 \frac{\rho}{\rho_s} \left(\frac{K_m - \rho_s c_s^2}{K_m - \rho c^2} \right) \left[e^{-2|\Gamma_s|d} \right] \right) \quad (2.15)$$

with the factor in [] omitted for $\theta > \theta_c$.

In Fig. 2.2, ΔTS is plotted as a function of θ for a frequency of 400 Hz and $d = 0.5\text{m}$ for the continental terrace sediment types (derived from Hamilton, 1980) listed in Table 1.1 assuming that $K_m = 0.8\rho c^2$. From Fig. 2 it is evident that the effect of target burial is an increase in target strength except at the very smallest grazing angles ($\theta < \sim 7^\circ$) for all sediment types. The increase in target strength is due to the increase in the contrast between the target compliance and the compliance of the scattering medium, and the fact that the magnitude of the transmission coefficient is greater than unity until $\theta \ll \theta_c$. (The compliance term will increase the target strength whenever the modulus of the target is closer to that of water than sediment.) These factors more than compensate for the density ratio term and the exponential decay term is insignificant when the burial depth is much less than a wavelength.

We apply Eq. (2.13) to a source with an arbitrary input pressure-time waveform given by

$$p_{source}(r, t) = p_0 \frac{r_0}{r} f(t - r/c) \quad (2.16)$$

to obtain our final result for the backscattered pressure from a buried object in the Rayleigh scattering regime:

$$p_{scat}(t) = \frac{-\rho}{4\pi} \frac{p_0 r_0}{r_m^2} V_m \left[\frac{\beta_m}{\rho_s c_s^2} \right] \left(\text{Re}(\hat{T}^2) \frac{\partial^2}{\partial t^2} f(t - 2r_m/c) + \text{Im}(\hat{T}^2) \frac{\partial^2}{\partial t^2} h(t - 2r_m/c) \right) F_R \quad (2.17)$$

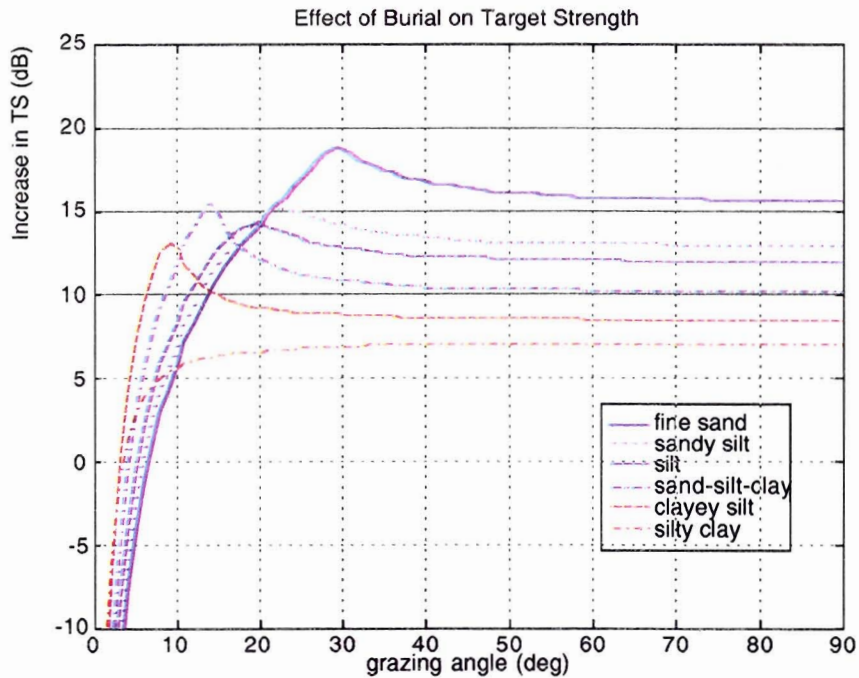


Figure 2.2. Effect of burial on target strength ($d = 0.5m$, $K_m = 0.8\rho c^2$, $f = 400$ Hz)

where $h(t)$ is the Hilbert transform of $f(t)$ and the small complex part of c_s is ignored in the term in []. It is difficult to rigorously include the evanescent exponential decay term which occurs in Eq. (2.13) when $\theta < \theta_c$ in the time dependent formulation. We have approximated its relatively insignificant effect, in the factor F_r in Eq. (2.17):

$$F_r = 1 \quad \text{for } \theta > \theta_c$$

$$F_r = e^{-|\Gamma_s \langle k_s \rangle d|} \quad \text{for } \theta < \theta_c$$
(2.18)

where $\langle k_s \rangle$ is the average wavenumber of the pulse.

Equation (2.17) could be used directly for some mines such as the MANTA which are reasonably well modeled as point Rayleigh scatterers. Most ground mines, however, are cylindrical in shape with rather large aspect ratios ($l \gg a$) and, as it stands, Eq. (2.17) would only be appropriate at broadside or at very low frequencies (typically < 100 Hz) where both ka and kl are small. As long as ka is small, the scattering from a cylinder can still be approximated by integrating (2.17). In (2.17) $p_{scat}(r_m)$ is the backscattered scattered pressure at the origin due to a volume scattering element V_m with compliance K_m which is located at a distance r_m from the source. Assume that a cylinder of length l and radius a is centered at \vec{r}_c and oriented in the direction \hat{e}_c . Each differential increment, dl , along the length of the cylinder can be considered to be a volume scatterer of modulus K_m with a differential volume $dV_m = \pi a^2 dl$. and the scattered pressure due to the entire cylinder is given by the integral

$$p_{cyl}(t) = \pi a^2 \int_{-l/2}^{l/2} p_{scat}(t, |\vec{r}_c + \hat{e}_c \xi|) d\xi$$
(2.19)

The maximum scattered pressure for a cylindrical mine occurs at broadside and is given by Eq. (2.17) with $V_m = \pi a^2 l$.

To include the effect of any density difference between the mine and the sediment we need to add a dipole term proportional to

$$\beta_d = \frac{3(\rho_m / \rho_s - 1)}{2\rho_m / \rho_s + 1} \quad (2.20)$$

where $\rho_m = M_m/V_m$ is the density of the mine. For backscatter, the induced dipole moment is in the direction of the receiver so there is no cosine factor in Eq. (2.20). For $kr_m \gg 1$ the density effect can be approximated by just replacing β_m by $\beta_m - \beta_d$ in Eq. (2.17):

$$p_{scat}(t) = \frac{-\rho}{4\pi} \frac{p_0 r_0}{r_m^2} V_m \left[\frac{\beta_m - \beta_d}{\rho_s c_s^2} \right] \left(\text{Re}(\hat{T}^2) \frac{\partial^2}{\partial t^2} f(t - 2r_m / c) + \text{Im}(\hat{T}^2) \frac{\partial^2}{\partial t^2} h(t - 2r_m / c) \right) F_r \quad (2.21)$$

In addition to the scattered pressure given above we may also need the horizontal components of the acoustic particle displacement. Euler's equation gives

$$\rho \frac{\partial^2 \vec{\xi}}{\partial t^2} = -\vec{\nabla} p \quad (2.22)$$

so from (2.21) the x -component of the acoustic particle displacement is given by

$$\xi_x(t) = \frac{x}{4\pi r_m} \left(\frac{p_0 r_0}{r_m^2} V_m \left[\frac{\beta_m - \beta_d}{\rho_s c_s^2} \right] \left(\frac{1}{r_m} + \frac{1}{c} \frac{\partial}{\partial t} \right) \left(\text{Re}(\hat{T}^2) f(t - \frac{2r_m}{c}) + \text{Im}(\hat{T}^2) h(t - \frac{2r_m}{c}) \right) F_r \right) \quad (2.23)$$

with a similar expression for the y -component.

3

Transmitted pulses and target echoes

Pulses

We require a short pulse in the frequency range from 200 to 500 Hz for our transmitted pressure signal. The pulse needs to be short to allow satisfactory localization of the mine. Since reverberation, not noise, is the limiting factor, long time-bandwidth product signals are of no help. A pressure waveform which has been found to be useful for scattering measurements is the *second derivative Gaussian*:

$$f_0(t) = [1 - 2(t/t_0 - 3)^2]e^{-(t/t_0 - 3)^2} \quad (3.1)$$

For our problem we choose $t_0 = 1$ msec. The top half of Fig. 3.1 shows f_0 (solid line) and its Hilbert transform, h_0 (dashed) plotted as functions of time. Note that f_0 is normalized so that its maximum value is unity. The bottom half of Fig. 3.1 shows the spectrum of f_0 which is seen to peak around 300 Hz. The function f_0 resembles a dolphin echo location click. The 3 dB down pulse width is approximately 0.6 msec.

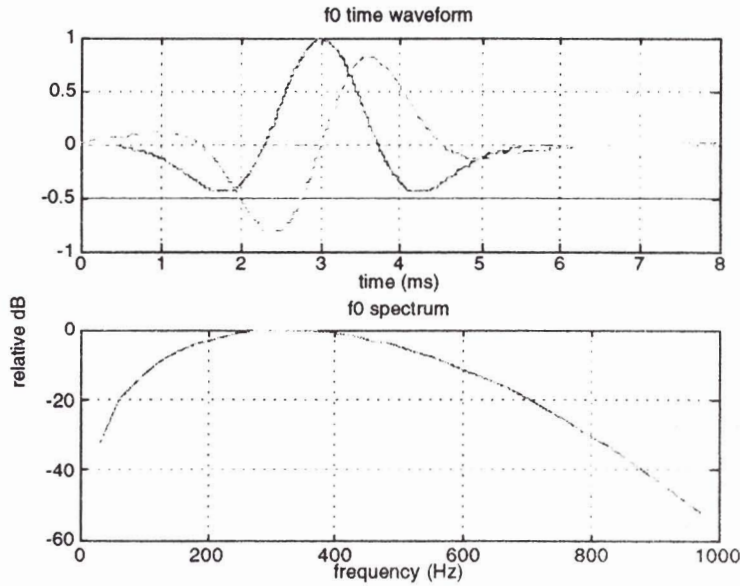


Figure 3.1 The function f_0 from Eq. (3.1) with $t_0 = 0.001$. Top: time waveform of $f_0(t)$ (solid line) and its Hilbert transform $h_0(t)$ (dashed line); bottom: spectrum of f_0 .

We shall also need certain derivatives of f_0 and h_0 . We designate these by

$$\begin{aligned} f_n &= \frac{d^n f_0}{dt^n} \\ h_n &= \frac{d^n h_0}{dt^n} \quad n = 0, 1, 2, \dots \end{aligned} \quad (3.2)$$

These functions are plotted in Fig. 3.2 for $t_0 = 1$ msec. Note that these functions have dimension t^n and differ widely in magnitude. The scattered pressure waveform is dominated by f_2 .

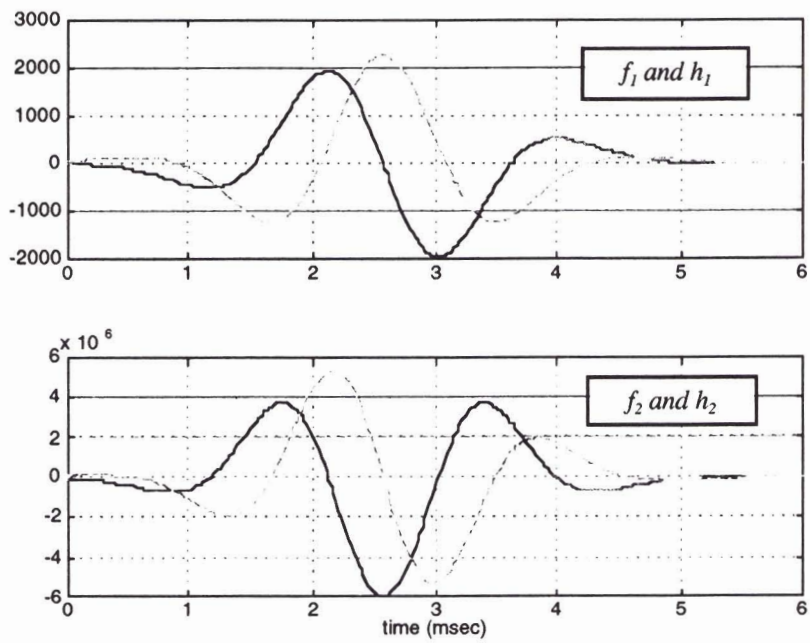


Figure 3.2. The functions f_n (solid line) and h_n (dashed lines) for $t_0 = 1$ msec.

In terms of these functions, the source pressure Eq. (2.16) is given by

$$p_{source}(r, t) = p_0 \frac{r_0}{r} f_0(t - r/c), \quad (3.3)$$

and Eq. (2.21) for the scattered pressure and Eq. (2.23) for the scattered displacement become

$$p_{scat}(t) = \frac{-\rho}{4\pi} \frac{p_0 r_0}{r_m^2} V_m \left[\frac{\beta_m - \beta_d}{\rho_s c_s^2} \right] \left(\text{Re}(\hat{T}^2) f_2(t') + \text{Im}(\hat{T}^2) h_2(t') \right) F_r \quad (3.4)$$

and

$$\xi_x(t) = \frac{x}{4\pi r_m} \frac{p_0 r_0}{r_m^2} V_m \left[\frac{\beta_m - \beta_d}{\rho_s c_s^2} \right] \left[\text{Re}(\hat{T}^2) \left(\frac{f_0(t')}{r_m} + \frac{f_1(t')}{c} \right) + \text{Im}(\hat{T}^2) \left(\frac{h_0(t')}{r_m} + \frac{h_1(t')}{c} \right) \right] \quad (3.5)$$

$$\text{where } t' = t - \frac{2r_m}{c}$$

It is necessary to produce a clean, high pressure level version of the pulse given by Eq. (3.3) (Fig. 3.1). In particular, it is necessary for the signal to terminate without any 'tail' since the echo is small (and in the proposed configuration rather early) and the receiver is close to the source. Even a small tail in the transmitted signal can overwhelm the echo. Broadband electrodynamic transducers such as the USRD¹ J series are incapable of producing satisfactory pulses. Such pulses, however, can be produced quite well using a piezoelectric source operated well below its resonance. Such a source produces a volume displacement which is proportional to the driving voltage and hence a radiated pressure

¹ USRD – Underwater Sound Reference Detachment, US Naval Underwater Warfare Centre, Orlando, Florida.

which is proportional to the second derivative of the drive voltage. The 25 in diameter ITC² spherical piezoelectric sources used at the ISMS³ at Lake Pend Oreille, are each capable of producing a 185 dB source level at 300 Hz with a 7000 V driving voltage. If driven with a Gaussian waveform (a waveform proportional to $f_2(t)$) with a peak voltage of 7000 V the resulting pressure will be given by Eq. (3.3) with a peak amplitude, p_0 , of 1000 Pa (180 dB source level) and no 'tail.' Such a source would be ideal for this application.

Mine parameters

The target strength of a mine depends primarily on its volume V_m and its stiffness K_m . Its volume cannot be any smaller than the volume of the desired explosive charge. The most lethal mines must have large volumes and hence proportionally large Rayleigh target strength. The stiffness of a mine is a less straightforward matter. In Fig 3.3 we plot TS vs target modulus K_m for the six sediment types. Assuming that the target stiffness comes entirely from the stiffness of the case (*i.e.* that the explosive provides little or no additional stiffness) the equivalent modulus is given by

$$K_m = \frac{Et}{2a} \quad (3.6)$$

where E is Young's modulus for the case material, t is its thickness and a is its radius. The assumption that K_m depends only on the case is not crucial to the development but, if it is valid, improves the likelihood that the mine has the desirable property of always being less compliant than the sediment. A low modulus is desirable because it can be used to distinguish mines from false targets (see Sect. 5) and, as can be seen from the figure, gives the mine a high TS in any sediment. Whether or not this assumption is valid depends on details of the mine construction and the mechanical properties of the explosive both of which are unknown to me. It seems a plausible enough assumption though, for most mines since they usually have some air-filled regions inside which are separated from the explosive by partitions which seem unlikely to be able to withstand high pressure. It therefore would seem necessary for the case to provide most of the stiffness of the mine. From Fig 3.3 we see that the target strength will be very low for any sediment whose modulus is closely matched to that of the mine.

² ITC – International Transducer Corporation.

³ ISMS – Intermediate Scale Measurement System, Acoustics Research Detachment, US Naval Surface Warfare Center, Bayview, Idaho.

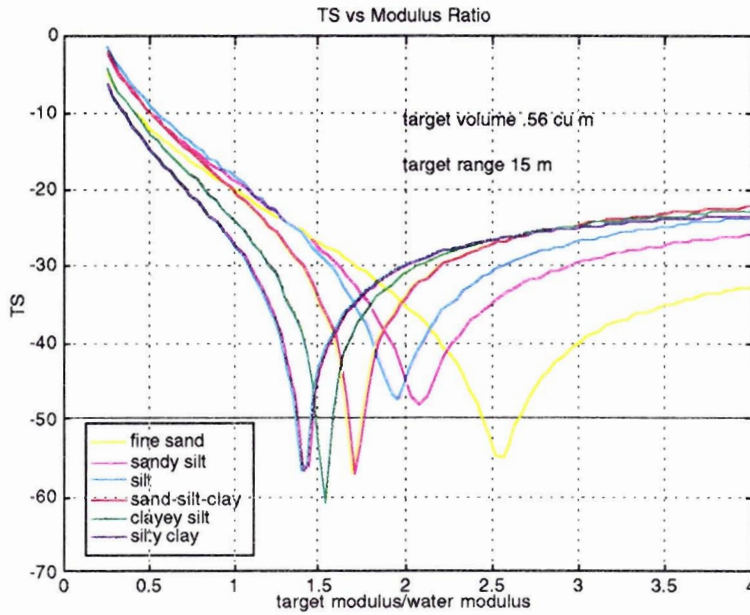


Figure 3.3 Target strength for a 0.56 m^3 target for different sediments and bulk modulus K_m

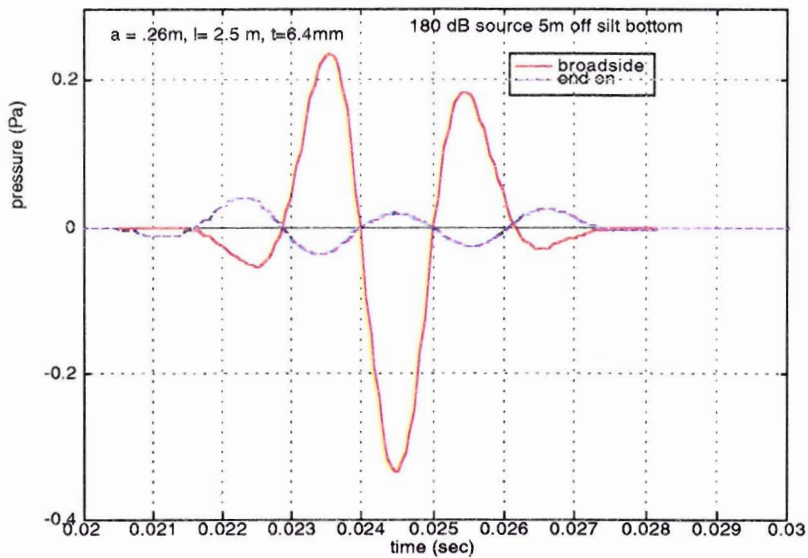


Figure 3.4 Broadside and end on echoes from a 2.5 m long target. Target has a 6.4 mm thick steel case and is buried 0.5m in the sediment.

Target echoes

The solid red line in Fig. 3.4 is a typical broadside target echo obtained from the model. Here the mine is assumed to be 1.27 cm steel cylinder 2.5 m long and 26 cm in radius buried 0.5 m. The sediment is silt, the range is 15 m and the source has a 180 dB source level and is 5 m from the bottom. Density difference effects are neglected. The shape of the waveform is predominantly $f_2(t)$. The target strength is -21 dB. Note that the side target echo has a 3 dB down width of only 0.5 msec. The end-on echo for this same target is shown by the blue dashed line in Fig. 3.4. It is much lower in amplitude and is more spread out. The end-on target strength is only -40 dB. A complete beam pattern for the target is shown in Fig. 3.5. The 3 dB down beamwidth is 34° and the 6 dB down beamwidth is approximately 50° . The directionality is not too severe and in any case, as mentioned earlier, as the sonar passes the mine, it must at some point be broadside to it.

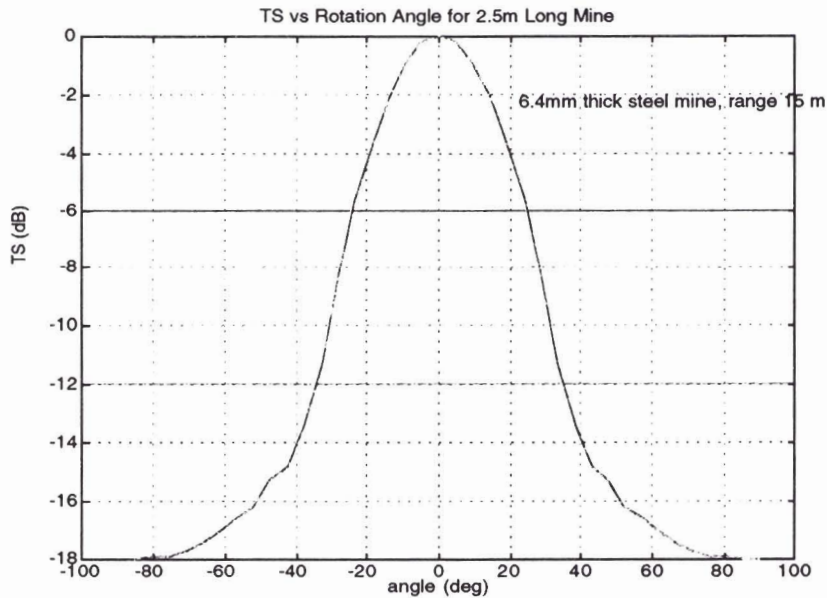


Figure 3.5 Target strength vs target rotation for the target of Fig. 3.

4

Reverberation

The reverberation consists of surface reverberation, bottom reverberation and volume reverberation. The surface reverberation, and the specular reflection from the surface are unimportant since, by design, they arrive much later than any echo of interest. They are important only in determining the allowable pulse repetition rate. Volume reverberation is, generally, quite small. The bottom reverberation, which is the limiting interference, consists of rough surface scatter and sediment volume scatter. We consider first reverberation due the roughness of the water/sediment interface.

One of the most commonly used and successful models for rough bottom backscatter is that of Jackson *et al.* (Jackson *et al.*, 1986, 1992; Mourad and Jackson, 1993). They employ a Rayleigh-Rice perturbation approach with composite roughness for small and medium grazing angles and use a Kirchhoff approximation for the steepest grazing angles ($>70^\circ$). We are not interested in steep angles since at the corresponding times any target echo would be overwhelmed by the direct and bottom reflected signals. Moreover, since the total bottom surface involved is quite small, there is no need for the 'composite roughness' approach. (The composite roughness model utilizes multiple scales. We have just one scale since the ranges and wavelengths are of comparable order. For the same reason shadowing effects cannot be important.) We are left with the Rayleigh-Rice part of Jackson's model which is essentially due to Kuo (1983). In this model, the backscattering from a bottom patch of area A is expressed in terms of a dimensionless 'scattering cross section' σ by

$$I_{scat} = \sigma I_0 A / r_A^2 \quad (4.1)$$

where I_0 and I_{scat} are the incident and scattered intensity and r_A is the distance between the receiver and the patch. The bottom is assumed to be isotropic with Gaussian statistics and a power law wavenumber spectrum. The two-dimensional roughness spectrum is given by

$$W(\kappa_x, \kappa_y) = \beta \left(\frac{1}{\sqrt{\kappa_x^2 + \kappa_y^2}} \right)^\gamma \quad (4.2)$$

where (κ_x, κ_y) is the two dimensional wavenumber vector. The quantity β which describes magnitude of the roughness, has dimensions m^4 , and has typical values ranging from 10^{-5} to 5×10^{-4} . The power law exponent γ has values between 3 and 4. The cross-section in the Kuo-Jackson model is given by

$$\sigma = 4k^4 \gamma_1^4 F(\gamma_1) W(2k\sqrt{1-\gamma_1^2}, 0) \quad (4.3)$$

where γ_1 is the sine of the grazing angle and $F(\gamma_1)$ is given by

$$F(\gamma_1) = \left(R_A(\gamma_1) + \frac{1-\gamma_1^2}{\gamma_1^2} R_B(\gamma_1) \right)^2 \quad (4.4)$$

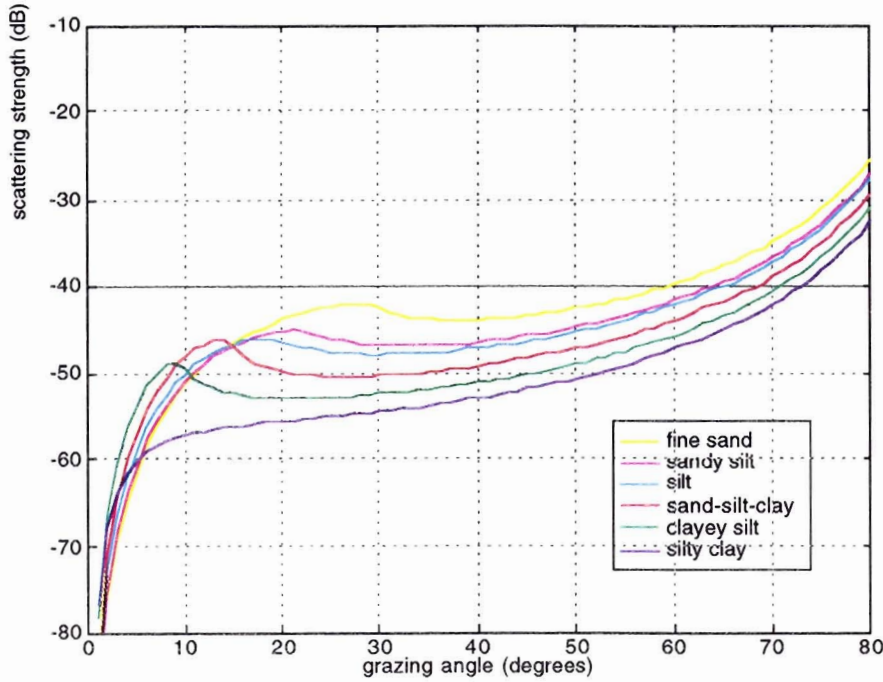


Figure 4.1 Bottom scattering strength from the Kuo-Jackson model for the six sediment types of Table 1.1 $f=350$ Hz and $\beta=0.0001 \text{ m}^4$

with R_A and R_B given by Eqs. (4.20) and (4.21). Note that σ is proportional to β and frequency to the $(4-\gamma)$ power. In Fig. 4.1, the ‘bottom scattering strength’, defined as $10\log_{10} \sigma$, is shown plotted as a function of grazing angle for each of the six sediment types shown in Table 1.1 for $\beta = 0.0001 \text{ m}^4$ at 350 Hz.

The expectation value for the total backscattered intensity as a function of time is obtained by integrating Eq. (4.1) over the appropriate area. In our case we have an omnidirectional source a distance z above the bottom. If the source level is $p_0 r_0$ and the pulse begins at $t=0$ and has length τ , the expectation value for the square of the scattered pressure is given by (see e.g. Carruthers, 1977)

$$\langle p_{scat}^2(z, t) \rangle = 2\pi p_0^2 r_0^2 \int_{w_{min}}^{w_{max}} \frac{\sigma(w / \sqrt{w^2 + z^2})}{(\sqrt{w^2 + z^2})^4} w dw \quad (4.5)$$

with the limits of integration given by

$$w_{\min} = \text{Re} \sqrt{\frac{c^2(t-\tau)^2}{4} - z^2} \quad (4.6)$$

$$w_{\max} = \text{Re} \sqrt{\frac{c^2 t^2}{4} - z^2} \quad (4.7)$$

Equation (4.5) could be used to estimated the reverberation for our problem. However, the Kuo-Jackson statistical approach to sediment scatter is questionable for our situation since it is implicitly assumed that the integration surface area for a given angle of incidence is large with respect to a wavelength, that we are in the farfield of the scattering region and that the total surface area is sufficiently large to express the assumed statistics. All of these assumptions are questionable in our case. However, because of the low frequencies and relatively short ranges involved, the problem is susceptible to a more direct solution. We can synthesize an ensemble of statistically valid realizations of the bottom and solve the deterministic time domain scattering problem for each realization. The ensemble of bottom scatter solutions (and its rms average) can then be compared with the predicted scattered signal from the mine to assess detectability of a given mine for a given bottom. The analysis proceeds by first determining the backscatter from a deterministic rough bottom.

Following Jackson, we base our model on the results of Kuo (1964) who carries out a perturbation analysis for the two-fluid case with sinusoidal plane waves. The incident plane wave is given by

$$p_{\text{inc}}(x, y, z, t) = p_{\text{pw}}(x, y, z, t) = \hat{p}_{\text{pw}} e^{ik(\alpha_1 x + \beta_1 y + \gamma_1 z)} e^{-i\omega t} \quad (4.8)$$

where α_1 , β_1 , and γ_1 are direction cosines and $k = \omega/c$.

Kuo shows that for a surface located at $z=0$ with a roughness given by $h(x, y) \ll \lambda$ the total field consists of an incident field, a specularly reflected field and a scattered field. Correct to first order in h the two-dimensional Fourier transform of the scattered field on the surface $z=0$ is given by

$$\tilde{p}_{scat}(k\alpha_2, k\beta_2) = \iint_S \left[\left(\frac{2ik\gamma_1^2}{\gamma_2} Q_A(\gamma_1, \gamma_2) h(\mathbf{r}_s) + \frac{Q_B(\gamma_1, \gamma_2)}{\gamma_2} \left(\alpha_1 \frac{\partial h}{\partial x_s} + \beta_1 \frac{\partial h}{\partial y_s} \right) \right) \hat{p}_{pw} e^{ik(\alpha_1 x_s + \beta_1 y_s)} \right] \times e^{-ik(\alpha_2 x_s + \beta_2 y_s)} dx_s dy_s \quad (4.9)$$

where

$$Q_A(\gamma_1, \gamma_2) = \frac{(\rho_s / \rho) \left[(\rho_s / \rho) - (c / \gamma_1 c_s)^2 \Gamma(\gamma_1)^2 \right] + (\rho_s / \rho - 1) (c / \gamma_1 c_s)^2 \Gamma(\gamma_1) \Gamma(\gamma_2)}{\left[(\rho_s / \rho) + (c / \gamma_1 c_s) \Gamma(\gamma_1) \right] \left[(\rho_s / \rho) + (c / \gamma_2 c_s) \Gamma(\gamma_2) \right]} \quad (4.10)$$

$$Q_B(\gamma_1, \gamma_2) = \frac{2(\rho_s / \rho)(\rho_s / \rho - 1)}{\left[(\rho_s / \rho) + (c / \gamma_1 c_s) \Gamma(\gamma_1) \right] \left[(\rho_s / \rho) + (c / \gamma_2 c_s) \Gamma(\gamma_2) \right]} \quad (4.11)$$

Surface points are denoted by $\mathbf{r}_s = (x_s, y_s)$ and α_2 , β_2 , and γ_2 are direction cosines for the scattered wave, and

$$\Gamma = \sqrt{1 - \frac{c_s^2}{c^2} (1 - \gamma^2)} \quad (4.12)$$

is the same as Γ_s in Eq. (2.5).

The term in brackets in Eq. (4.9) can be regarded as a pressure source term for the scattered signal. In accordance with the perturbation approach this term is first-order in the perturbation quantities h , $\partial h/\partial x$ and $\partial h/\partial y$. The term in brackets is not completely analogous to a source term since it depends on the field coordinates through the γ_1 term. This is probably a consequence of the fact that the rough surface perturbs not only the incident and reflected signals but the Green's function for the plane surface as well. The consequences of treating the bracketed term as a source term will be seen shortly. From the Helmholtz integral and Eq. (4.9), if we assume that the region where h and its derivatives are nonzero is finite, in the farfield of this region the pressure is given by

$$\begin{aligned}
 p_{scat}(r, \alpha_2, \beta_2, t) &= \frac{e^{i(kr - \alpha t)}}{2\pi r} \iint_S \left[\left(\frac{2ik\gamma_1^2}{\gamma_2} Q_A h(\mathbf{r}_s) + \frac{Q_B}{\gamma_2} \left(\alpha_1 \frac{\partial h}{\partial x_s} + \beta_1 \frac{\partial h}{\partial y_s} \right) \right) \hat{p}_{pw0} e^{ik(\alpha_1 x_s + \beta_1 y_s)} \right] \\
 &\quad \times (ik\gamma_2) e^{-ik(\alpha_2 x_s + \beta_2 y_s)} dx_s dy_s \\
 &= \frac{e^{ikr}}{2\pi r} \iint_S \left[2Q_A(\gamma_1, \gamma_2) h(\mathbf{r}_s) \frac{\partial^2 p_{pw}}{\partial z_s^2} + Q_B(\gamma_1, \gamma_2) \left(\frac{\partial h}{\partial x_s} \frac{\partial p_{pw}}{\partial x_s} + \frac{\partial h}{\partial y_s} \frac{\partial p_{pw}}{\partial y_s} \right) \right] \\
 &\quad \times e^{-ik(\alpha_2 x_s + \beta_2 y_s)} dx_s dy_s
 \end{aligned} \tag{4.13}$$

where r is the distance from the center of the region to the far field observation point. The assumption that h is zero beyond some range is reasonable since we will eventually be dealing with finite length pulses and finite length receive windows. Any part of the bottom which is so far away from the source that its reverberation falls outside the receive window might just as well have zero roughness. Any field point (x_F, y_F, z_F) is in the farfield of any given infinitesimal portion of the surface. Thus from Eq. (4.13), the contribution to the pressure at the point (x_F, y_F, z_F) due to the surface area element $dx_s dy_s$ located at $(x_s, y_s, 0)$ is given by

$$dp_{scat}(\mathbf{r}_F, t) = \frac{e^{ikr'}}{2\pi r'} \left[\left(2Q_A \left(\gamma_1, \frac{z_F}{r'} \right) h(x_s, y_s) \frac{\partial^2 p_{pw}}{\partial z_s^2} + Q_B \left(\gamma_1, \frac{z_F}{r'} \right) \left(\frac{\partial h}{\partial x_s} \frac{\partial p_{pw}}{\partial x_s} + \frac{\partial h}{\partial y_s} \frac{\partial p_{pw}}{\partial y_s} \right) \right) \right] dx_s dy_s \tag{4.14}$$

where r' is the distance between the source point and the field point:

$$r' = \sqrt{(x_F - x_S)^2 + (y_F - y_S)^2 + z_F^2} \quad (4.15)$$

It is recognized dp_{scat} in Eq. (4.14) does not satisfy the wave equation exactly because of the r' dependence of Q_A and Q_B . For our case, however, Q_A and Q_B are much weaker functions of the field coordinates than is $\exp(ikr')/r'$ (and especially so far away from the critical angle) so the product does satisfy the wave equation approximately.

In a similar fashion, we can replace the plane wave incident signal with a spherical wave incident signal, Eq. (2.2), radiated from a projector located at (x_P, y_P, z_P) . With the appropriate modification of Q_A and Q_B , Eq. (4.14) becomes

$$\begin{aligned} dp_{scat}(\mathbf{r}_F, t) = \frac{\hat{p}_0 r_0}{2\pi} \left(\frac{e^{ikr'}}{r'} \right) \left[2Q_A \left(\frac{z_P}{r''}, \frac{z_F}{r'} \right) h(x_S, y_S) \frac{\partial^2}{\partial z_S^2} \left(\frac{e^{ikr''}}{r''} \right) \right. \\ \left. + Q_B \left(\frac{z_P}{r''}, \frac{z_F}{r'} \right) \left(\frac{\partial h}{\partial x_S} \frac{\partial}{\partial x_S} + \frac{\partial h}{\partial y_S} \frac{\partial}{\partial y_S} \right) \left(\frac{e^{ikr''}}{r''} \right) \right] dx_S dy_S \end{aligned} \quad (4.16)$$

where

$$r'' = \sqrt{(x_P - x_S)^2 + (y_P - y_S)^2 + z_P^2} \quad (4.17)$$

The scattered field is obtained by integrating Eq. (4.16) over S . We are interested in the backscattered case $(x_P, y_P, z_P) = (x_F, y_F, z_F)$. We choose the source and receiver to be located at $(0, 0, z)$, so

$$r' = r'' = \sqrt{x_S^2 + y_S^2 + z^2} = \sqrt{r_S^2 + z^2} \quad (4.18)$$

and the scattered pressure is given by

$$p_{scat}(z,t) = \frac{\hat{p}_0 r_0}{2\pi} \iint_S \left(\frac{e^{i(kr' - \omega t)}}{r'} \right) \left[2R_A \left(\frac{z}{r'} \right) h(\mathbf{r}_s) \frac{\partial^2}{\partial z_s^2} \left(\frac{e^{ikr'}}{r'} \right) + R_B \left(\frac{z}{r'} \right) \left(\frac{\partial h}{\partial x_s} \frac{\partial}{\partial x_s} + \frac{\partial h}{\partial y_s} \frac{\partial}{\partial y_s} \right) \left(\frac{e^{ikr'}}{r'} \right) \right] dx_s dy_s \quad (4.19)$$

where from Eqs. (4.10) and (4.11) the functions R_A and R_B are given by

$$R_A(\gamma) = \frac{(\rho_s / \rho) - (c / \chi_s) \Gamma(\gamma)}{(\rho_s / \rho) + (c / \chi_s) \Gamma(\gamma)} \quad (4.20)$$

$$R_B(\gamma) = \frac{2(\rho_s / \rho)(\rho_s / \rho - 1)}{[(\rho_s / \rho) + (c / \chi_s) \Gamma(\gamma)]^2} \quad (4.21)$$

Note that R_A is just the Rayleigh reflection coefficient for the two-fluid problem.

Expanding the indicated partial derivatives in Eq. (4.19) we obtain

$$p_{scat}(z,t) = \frac{\hat{p}_0 r_0}{2\pi} \iint_S \left(\frac{e^{i(2kr' - \omega t)}}{r'^2} \right) \left[2R_A \left(\frac{z}{r'} \right) h(\mathbf{r}_s) \left(\frac{-k^2 z^2}{r'^2} + \frac{ik(r_s^2 - z^2)}{r'^3} - \frac{(r_s^2 - 2z^2)}{r'^4} \right) \right. \\ \left. + R_B \left(\frac{z}{r'} \right) \left(\frac{\partial h}{\partial x_s} \frac{x_s}{r'} + \frac{\partial h}{\partial y_s} \frac{y_s}{r'} \right) \left(ik - \frac{1}{r'} \right) \right] dx_s dy_s \quad (4.22)$$

The transformation from a cw incident wave to a pulse is easy to make. From the argument of the exponential term in Eq. (4.22), the time functions are to be evaluated at the retarded time $t - 2r'/c$. Terms which have multipliers of ik involve the time derivative of the time function and terms which have multipliers of k^2 will involve second time derivatives. For our second-derivative Gaussian pressure incident waveform, $f_0(t)$ given by Eq. (3.1), the backscattered pressure becomes

$$p_{scat}(z,t) = \frac{\hat{p}_0 r_0}{2\pi} \text{Re} \iint_S \left[2 \frac{R_A(z/r')}{r'^2} h(\mathbf{r}_s) \left(\frac{z^2}{c^2 r'^2} f_2(t - \frac{2r'}{c}) - \frac{(r_s^2 - 2z^2)}{c r'^3} f_1(t - \frac{2r'}{c}) - \frac{(r_s^2 - 2z^2)}{r'^4} f_0(t - \frac{2r'}{c}) \right) \right. \\ \left. - \frac{R_B(z/r')}{r'^2} \left(\frac{z}{r'} \right) \left(\frac{\partial h}{\partial x_s} \frac{x_s}{r'} + \frac{\partial h}{\partial y_s} \frac{y_s}{r'} \right) \left(f_1(t - \frac{2r'}{c}) + \frac{1}{r'} f_0(t - \frac{2r'}{c}) \right) \right] dx_s dy_s \\ + \frac{\hat{p}_0 r_0}{2\pi} \text{Im} \iint_S \left[2 \frac{R_A(z/r')}{r'^2} h(\mathbf{r}_s) \left(\frac{z^2}{c^2 r'^2} h_2(t - \frac{2r'}{c}) - \frac{(r_s^2 - 2z^2)}{c r'^3} h_1(t - \frac{2r'}{c}) - \frac{(r_s^2 - 2z^2)}{r'^4} h_0(t - \frac{2r'}{c}) \right) \right. \\ \left. - \frac{R_B(z/r')}{r'^2} \left(\frac{z}{r'} \right) \left(\frac{\partial h}{\partial x_s} \frac{x_s}{r'} + \frac{\partial h}{\partial y_s} \frac{y_s}{r'} \right) \left(h_1(t - \frac{2r'}{c}) + \frac{1}{r'} h_0(t - \frac{2r'}{c}) \right) \right] dx_s dy_s \quad (4.23)$$

The expression is evaluated by numerical integration over an area of $40 \text{ m} \times 40 \text{ m}$. The integration goes fairly quickly because the pulse is relatively short and not rapidly varying.

We evaluate Eq. (4.23) for an ensemble of synthesized values for $h(x_s, y_s)$ which are characteristic of the bottom under consideration. The sample values for $h(x_s, y_s)$ are synthesized by taking two-dimensional white Gaussian noise, transforming it into wavenumber space, shaping it with the roughness spectrum Eq. (4.2), and transforming

back to space coordinates. The resulting ensemble is checked to make sure that the resulting structure function (Jackson *et al.*, 1986) is correct. A typical synthesized bottom is shown in Fig. 4.2. Note the 2:1 exaggeration in height to lateral dimension.

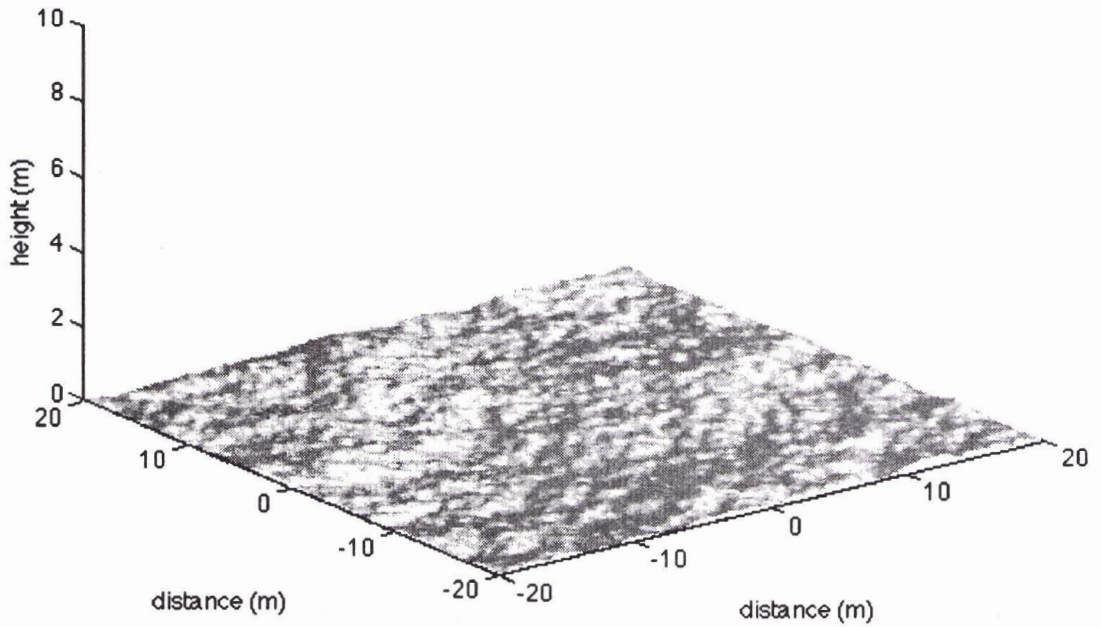


Figure 4.2 Example of synthesized rough bottom $\beta=0.0001$, $\gamma=3.25$

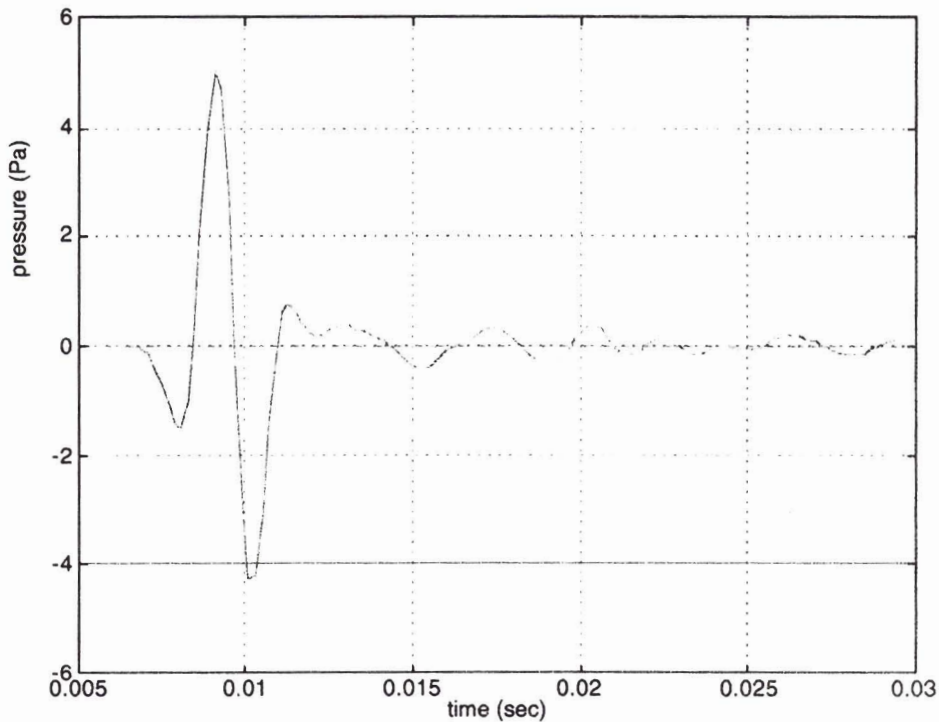


Figure 4.3 Sample backscattered pressure waveform from rough sand bottom
 $\beta=0.0001$, $\gamma=3.25$ (180 dB source, 5 m off bottom)

The backscattered pressure for this bottom with a sand sediment and a 180 dB source 5 m off the bottom is shown in Fig. 4.3. The large signal at the beginning which looks like the first derivative of the incident signal is typical. It is a consequence of the fact that the rough surface alters the arrival time of the reflected pulse. The derivative shaped scattered signal when added to the reflected signal has the effect of displacing it in time. This large signal is of no significance since it is windowed out along with reflected signal. The entire ensemble of 40 waveforms is shown in Fig. 4.4. The pressure after 0.0175 sec has been multiplied by 10 for clarity. Note the large coherent signals at early times but that later the pressure waveforms become small and incoherent

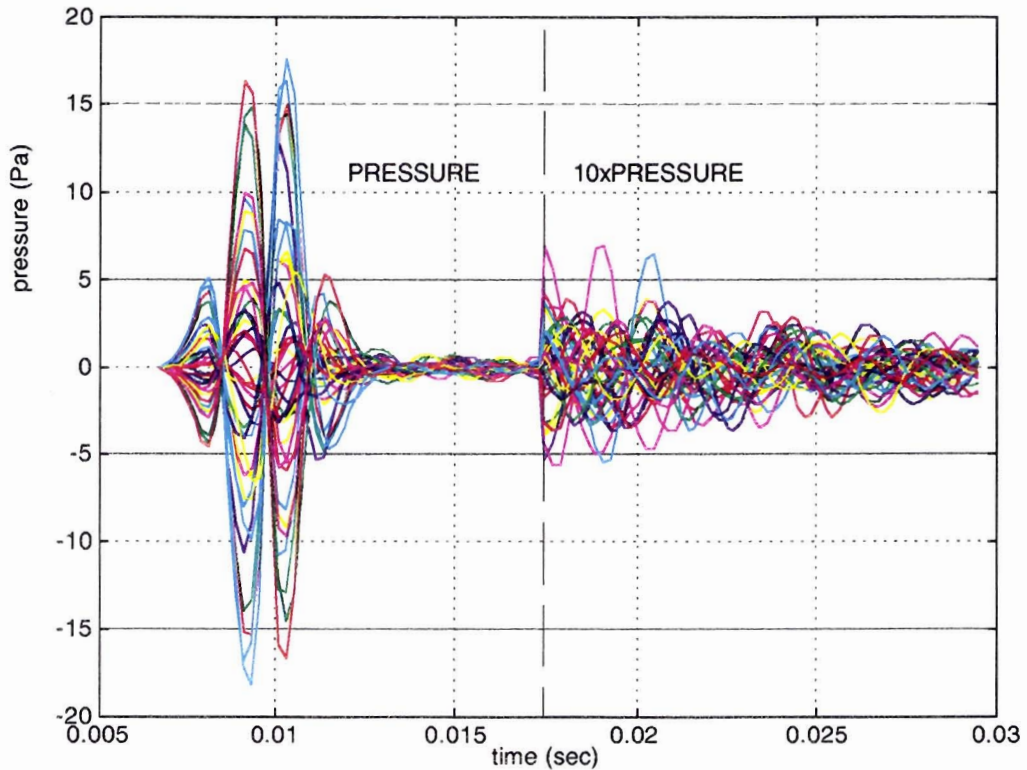


Figure 4.4 Backscattered pressure waveform for 40 synthesized samples of sand bottom
 $\beta = 0.0001$, $\gamma = 3.25$ (180 dB source, 5 m off bottom)

The expectation value for the rms scattered pressure is found by calculating the rms value of an 80 sample ensemble at each time point. The result for five sediment types is shown Fig. 4.5 along with the corresponding values predicted by the Kuo-Jackson model, Eq. (4.5). The Kuo-Jackson model does reasonably well in the region of interest. The Kuo-Jackson model, however, predicts reverberation levels 1–5 dB higher than those predicted by Eq. (4.23) even though the pulse length, τ , used in the calculation was the 3 dB down pulse width, the smallest justifiable value for this parameter.

Sediment volume scatter

Unlike the sediment surface scatter which is easily modeled in terms of known sediment and topographic parameters volume scatter is a rather *ad hoc* phenomena which is often

described in terms of an empirical volume scattering coefficient σ_v without regard to the physical scattering process. It is not currently possible to determine *a priori* the effect of sediment volume scatter on the proposed system. We believe, however, sediment volume backscatter is not the dominant mechanism for our situation.

1. When sediment volume backscatter dominates the reverberation it is usually because, due to low sediment sound attenuation, noncritical scattering and weak sound speed gradients in the sediment, there is significant penetration of sound into the sediment (tens or even hundreds of meters). If the surface which contributes to the sediment surface scatter at a given time is a ring of area $A (= 2\pi \times \text{range} \times \text{pulse length})$ the volume which contributes to the sediment volume reverberation is assumed to be a cylindrical shell of volume $A \times \text{penetration depth}$. For our situation however the scattering volume is actually a spherical cap which for the relevant geometry should be much smaller. This geometrical effect can be easily accounted for if σ_v can be estimated.
2. According to Jackson's model (Mourad and Jackson, 1993), σ_v depends on frequency to only the first power. If the scattering coefficient is that frequency independent then the scale of the relevant scatterers must be large with respect to a wavelength and therefore cannot be well defined on the scale of our system which is only a few wavelengths. Moreover, according to Jackson (1986): 'For centimeter length acoustic waves, it is likely that the most important inhomogeneity is not the graininess of the sediment, but larger scale inhomogeneities such as those caused by burrowing and shells.' It is difficult to see how inhomogeneities of biological origin can be extrapolated to meter scale acoustic waves, especially when they must extend tens or even hundreds of meters into the sediment.
3. Lyons et al. (1994) model the sediment volume scatter based on measured inhomogeneity of the sediment. For their case (6500 Hz) they find that the sediment volume scatter term dominates by about 15 dB. In Fig. 4.6 we plot the Lyons' et al. for σ_v as a function of frequency. It is quite evident that in our frequency range σ_v is proportional to frequency to the fourth power not linearly with frequency as per Jackson. The scattered pressure which is proportional to ω^2 would be more than 45 dB lower for our frequency band. From Fig. 4.6, at our midband frequency of 350 Hz, $\sigma_v = 4 \times 10^{-7}$. From Jackson's low-frequency results (1993) we can infer values for σ_v of 2.4×10^{-8} , 2.8×10^{-7} , 4.2×10^{-7} , 4.8×10^{-7} and 2.8×10^{-5} at 350 Hz – remarkable, but undoubtedly coincidental, agreement considering the vast difference in frequency dependence. We use Lyons' value of $\sigma_v = 4 \times 10^{-7}$ in a very simple model for sediment volume backscatter which neglects refraction, transmission and attenuation effects, and compare the results with our surface reverberation results (Fig. 4.5) in Fig. 4.7. The volume scattering is seen to be relatively unimportant. One should not read too much

into this result, but it does show that it is possible that sediment volume effects may be unimportant for our situation, even in regions where sediment volume effects have been shown to dominate in other experiments.

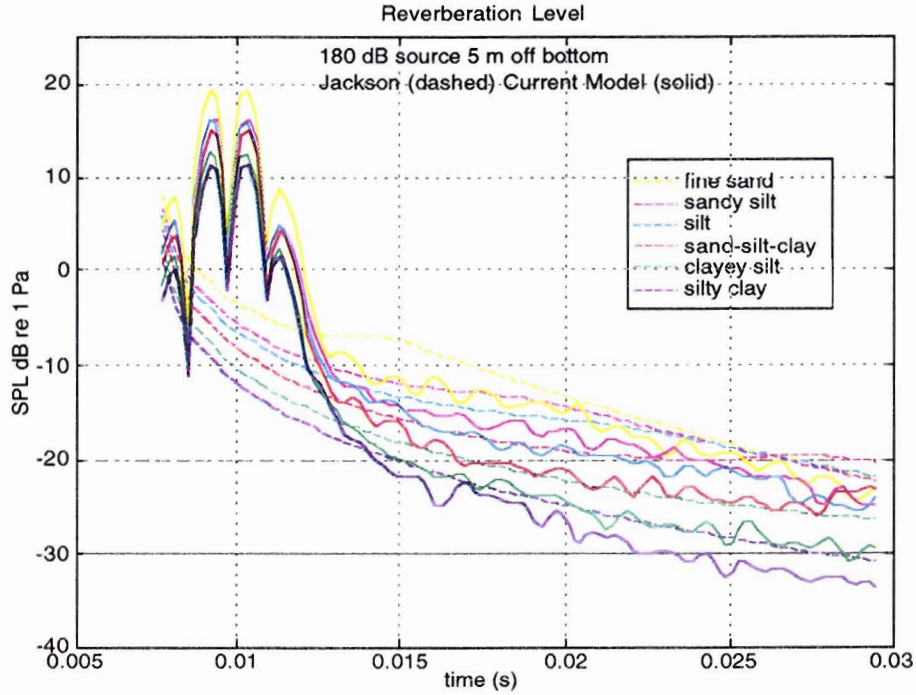


Figure 4.5 Predicted mean reverberation for five sediment types for a 180 dB source, $z = 5\text{ m}$; solid line – current model (80 sample ensemble); dashed line – Kuo-Jackson model

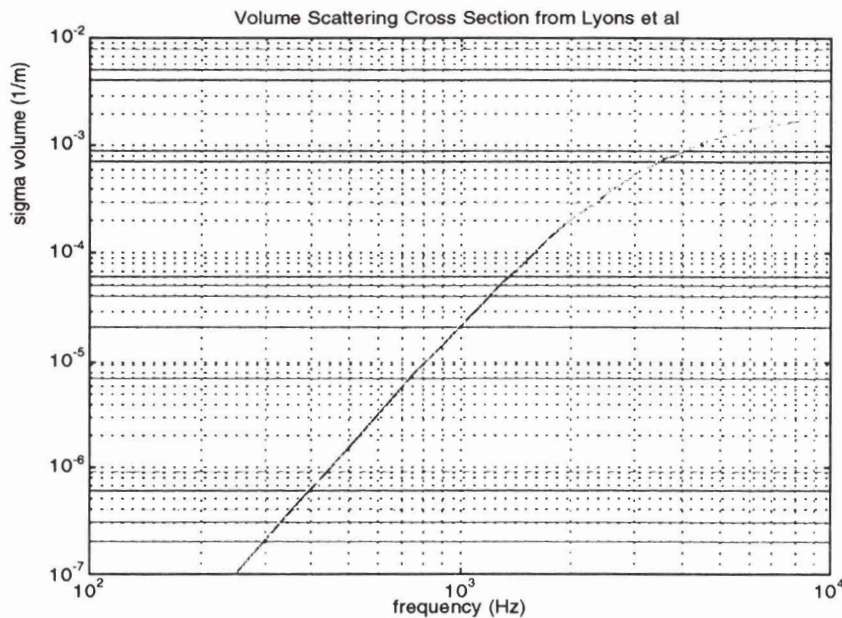


Figure 4.6 Sediment volume scatter coefficient σ_v from Lyons and Anderson (1994)

4. It is also possible that what people have been attributing to sediment volume scatter is in fact the result of rough surface scatter from some underlying rough sediment layer interface. If such a layer lies deep within the bottom the scattering from such surfaces would be unimportant for our case (but important in a long-range experiment) because in our case they would be gated out along with the reflections from the interface.

Though it is plausible that sediment volume scatter does not usually dominate the reverberation for our system, it can by no means be proven or even convincingly demonstrated. The importance of sediment volume scatter remains a major uncertainty which will have to be resolved experimentally.

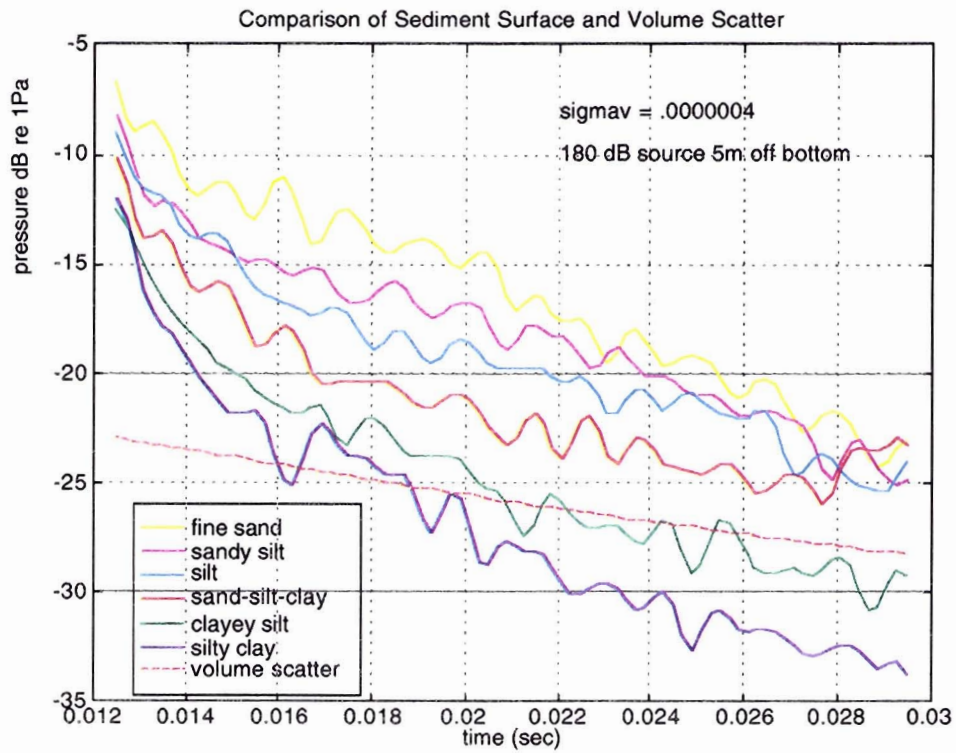


Figure 4.7 Sediment volume backscatter using Lyons' and Anderson's ($\sigma_v = 4 \times 10^{-7}$) (dashed line) compared with the surface backscatter results of Fig. 4.5

5

Detectability of buried mines

The results of the previous sections can be utilized to assess the detectability of a buried mine for a given scenario. For example, suppose we have a 53.3 cm (21 in) diameter, 2.5 m long cylindrical mine with a 6.4 mm (1/4 in) steel shell buried 0.5 m deep in a silt sediment. We use the results of Sect. 3 with a volume of 0.56 m^3 to determine the broadside backscattered echo at a lateral range of 15 m from a 180 dB source 5 m off the bottom. We assume that the mine's stiffness is determined solely by the case, use a Young's modulus of 220 GPa for steel and neglect any density differences. We use the results of Sect. 4 to obtain the reverberation. We assume a power law roughness spectrum with $\beta = 0.0001$ and $\gamma = 3.25$ to create an ensemble of forty $40 \text{ m} \times 40 \text{ m}$ bottoms and calculate the back scattered pressure for each. The magnitude of the resulting pressures are plotted in Fig. 5.1. The scattered signal is clearly detectable in all cases. (Depending on the threshold chosen there may also be a potential false detection at 0.02 sec.)

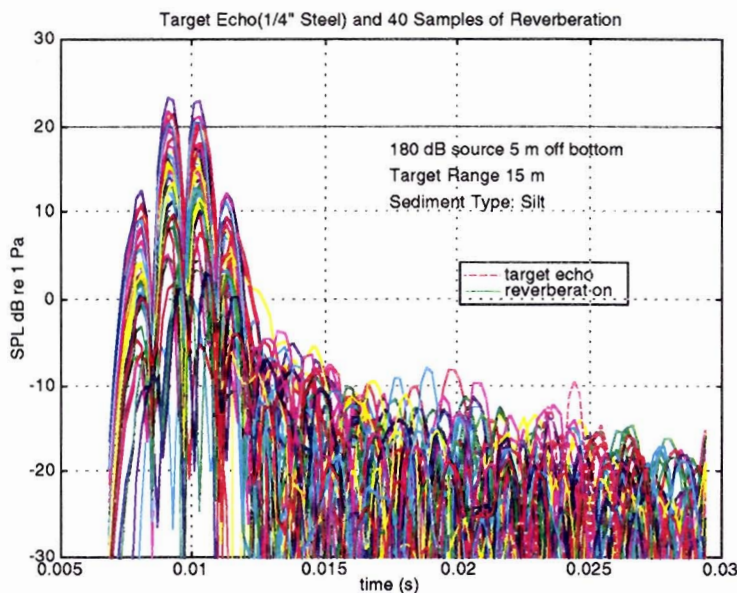


Figure 5.1 Target echo SPL compared with reverberation from 40 samples of a rough silt bottom $\beta=0.0001$, $\gamma=3.25$

A more useful comparison, however, is between the target echo and the rms ensemble average of the 40 sample reverberation signals. This is shown in Fig. 5.2. The signal for this case, is seen to be 12 dB above the mean reverberation level.

A more general plot is shown in Fig. 5.3 which compares the peak pressure of a 25 dB TS target echo with the reverberation for five sediment types. Other target strengths (e.g. taken from Fig. 3.3) could be used with appropriate adjustments. The reverberation calculation assumes $\beta = 0.0001$, but other roughness values could be used by making use of the fact that the reverberation is proportional to the square root of β .

The detectability of a buried mine depends on the signal excess, the difference in dB between the signal (target echo level) and the reverberation level. The signal-to-reverberation level, can be directly related to detection and false alarm rates, since the reverberation at a given range is a zero mean Gaussian quantity and the maximum echo is deterministic. In Table 5.1 signal-to-reverberation is shown for a buried ($d=0.5\text{m}$) mine with eight case thickness ranging from 6.4 to 25.4 mm (1/4 in to 1 in) made of three different case materials, steel, aluminum and glass reinforced epoxy (Young's modulus of 220, 72 and 34 GPa, respectively). The mine is assumed to be broadside and to have a volume of 0.56 m^3 which is the volume of a 53 cm (21 in) diameter, 2.5 m long mine. Other mine volumes can be accommodated by adding $20\log_{10}(V_m/.56)$ to the tabulated numbers since the echo is proportional to V_m . Other target orientations can be evaluated using the beam pattern given in Fig. 3.5. The reverberation level is calculated for $\beta = 0.0001$. Reverberation levels for other values of β can be easily obtained by subtracting $10\log_{10}(\beta/.0001)$. Note that for all but 12 cases (which are highlighted in the table) the signal-to-reverberation ratio is positive. In order to make trends clearer, the data in Table 5.1 is retabulated in Table 5.2 in order of increasing target bulk modulus. Signal excess can also be determined from Figs. 5.3 and 3.3 in the manner indicated earlier. Signal-to-reverberation level can be improved by averaging over multiple pulses or array averaging over times/distances sufficiently large for the bottom scatter to be incoherent. Perhaps an additional 6 dB could be achieved in this way without adding too much complexity to the system.

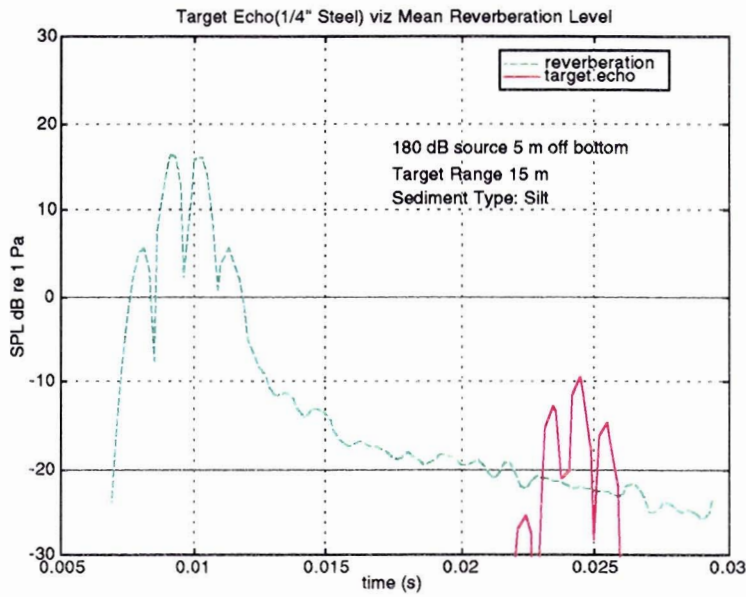


Figure 5.2 Target echo SPL compared with the rms average of the reverberation from 40 samples of a rough silt bottom $\beta=0.0001$, $\gamma=3.25$

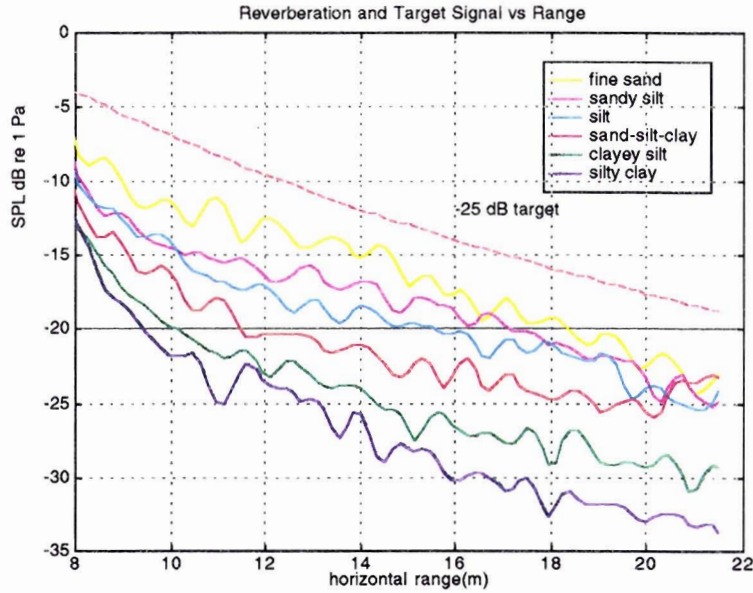


Figure 5.3 Reverberation compared with a -25dB TS target echo as a function of horizontal range

Table 5.1 Signal-to-reverberation for 5 sediment types and 21 mine configurations (mine volume 0.56 m^3 , $\beta=0.0001$, $\gamma=3.25$)

Signal-to-Reverberation Level (dB)							
Mine			Sediment				
Material	Thickness (mm)	Modulus Ratio	Fine Sand	Sandy Silt	Silt	Sand-Silt Clay	Clayey Silt
Al	6.4	0.381	22	26	28	29	31
Al	9.5	0.571	18	21	24	24	26
Al	12.7	0.762	14	17	20	20	22
Al	15.9	0.952	11	14	16	16	17
Al	19.1	1.143	9	11	13	12	12
Al	22.2	1.333	6	7	9	7	5
Al	25.4	1.524	4	4	5	0	-22
Steel	6.4	1.164	8	10	13	12	12
Steel	9.5	1.746	0	-2	-2	-14	4
Steel	12.7	2.328	-13	-6	1	7	12
Steel	15.9	2.910	-11	2	7	11	15
Steel	19.1	3.492	-4	5	9	12	17
Steel	22.2	4.074	-2	6	10	14	18
Steel	25.4	4.656	0	8	11	14	18
GRE	6.4	0.201	28	32	35	36	38
GRE	9.5	0.302	24	28	31	32	34
GRE	12.7	0.402	22	25	28	28	31
GRE	15.9	0.503	19	22	25	26	28
GRE	19.1	0.603	17	20	23	24	25
GRE	22.2	0.704	15	18	21	21	23
GRE	25.4	0.804	14	17	19	19	21

Table 5.2 Same as Table 5.1 but sorted by modulus

			Signal-to-Reverberation Level (dB)				
Mine			Sediment				
Material	Thickness (mm)	Modulus Ratio	Fine Sand	Sandy Silt	Silt	Sand-Silt Clay	Clayey Silt
GRE	6.4	0.201	28	32	35	36	38
GRE	9.5	0.302	24	28	31	32	34
Al	6.4	0.381	22	26	28	29	31
GRE	12.7	0.402	22	25	28	28	31
GRE	15.9	0.503	19	22	25	26	28
Al	9.5	0.571	18	21	24	24	26
GRE	19.1	0.603	17	20	23	24	25
GRE	22.2	0.704	15	18	21	21	23
Al	12.7	0.762	14	17	20	20	22
GRE	25.4	0.804	14	17	19	19	21
Al	15.9	0.952	11	14	16	16	17
Al	19.1	1.143	9	11	13	12	12
Steel	6.4	1.164	8	10	13	12	12
Al	22.2	1.333	6	7	9	7	5
Al	25.4	1.524	4	4	5	0	-22
Steel	9.5	1.746	0	-2	-2	-14	4
Steel	12.7	2.328	-13	-6	1	7	12
Steel	15.9	2.910	-11	2	7	11	15
Steel	19.1	3.492	-4	5	9	12	17
Steel	22.2	4.074	-2	6	10	14	18
Steel	25.4	4.656	0	8	11	14	18

Ambient noise

In an active sonar the ambient noise determines the required source level of the projector. If possible, the source level should always be increased until the reverberation rather than the ambient noise becomes the limiting interference. A reasonable, high-end, benchmark ambient noise level for the 200 to 500 Hz band is 72 dB *re* 1Pa/ $\sqrt{\text{Hz}}$ (Jensen *et al.*, 1994, p. 59). The rms noise pressure level is thus

$$SPL_{\text{noise}} = 72 + 10\log_{10}(\Delta f) = 96\text{dB} \quad (5.1)$$

and the signal excess is

$$SE = TS + SL - 40\log_{10} R - SPL_{\text{noise}} \quad (5.2)$$

Thus, at this noise level, with a 180 dB source, a -30 dB TS and a 6 dB SE, the ambient noise would limit detection range to 15 m for a single pulse and a single sensor. Averaging over eight pulses would be required to extend to range to the nominal 25 m. This may not be achievable with an acceptable rate of advance unless the allowable pulse repetition rate is high which is not likely. Most likely, the range would in fact be limited to 15 m under these circumstances. The possibility of using a small horizontal array of sensors to improve the SNR should also be considered but the short range of the system (relative so the acoustic wavelength), however, severely limits achievable directivity index. It is also evident that the use of a 180 dB source, such as the ITC ISMS sphere, is not extravagant.

False targets

Most submerged objects with the exception of trapped air bubbles like the swim bladders of fish and the lungs of marine mammals are stiffer than water. For such objects, the echo strength, like that of a mine is proportional to the volume and frequency squared with coefficients that cannot be too different than those of a mine. Basically, it takes an object as large as a mine to have a low-frequency echo as big as a mine's. Moreover, if it turns out that a mine's modulus is always (usually?) less than that of the sediment, the polarity of the signal will differentiate such false targets from mines (*i.e.* the mine echo will be inverted.)

Finally, the detection zone, is sufficiently small, so that that under many circumstances it should be possible to visually identify non-buried false targets.

Air bubbles have a TS of $20\log(a/2r_0)$ above resonance, a very high TS at resonance and Rayleigh scatter below resonance. At resonance, however, the signal from a bubble would be easily discernible by its long tail. Above resonance a bubble would have to have a radius of 6 cm to have a -30 dB TS. This is a rather large bubble to be found at the bottom of the ocean. The radius of a bubble with a resonance frequency of 350 Hz is only about 1 cm (Pierce, 1981, p. 438). The volume of a bubble whose resonance frequency is below 350 Hz below is so much smaller than a mine's (less than $4 \times 10^{-6} \text{ m}^3$ vs 0.56 m^3 for a mine) that even though it is much more compliant than a mine (bulk modulus 138 kPa vs 3 GPa) its target strength, below resonance, is much smaller than that of a mine.

As mentioned in Sect. 1, reflections from subbottom layers can be discriminated against by using horizontal acoustic motion sensors.

6

Conclusions and recommendations

The study has shown that it may be possible to detect buried mines using Rayleigh scattered second-derivative-Gaussian pulses in the 200–500 Hz band ($t_0 = 1$ msec). There are not many dB to spare and much uncertainty remains.

1. The target echo model should be valid but information is lacking on the detailed structure of the mines and the mechanical properties of the explosives needed to determine the bulk modulus (K_m) required by the model. Mine density has also only been estimated
2. The nearfield rough surface scattering model looks promising but needs to be validated.
3. The importance or lack of importance of sediment volume scattering for this problem needs to be ascertained.

A simple experiment could probably determine whether or not this approach to buried mine detection is viable. The experiment would consist of measuring short range echoes of buried mines or certifiably mine-like objects using second-derivative-Gaussian pulse and measuring the nearfield reverberation in a couple of representative sites where the bottom roughness parameters are known. In addition engineering issues regarding optimal configuration, use of arrays, signal processing, search strategy and platform considerations need to be resolved.

References

-
- Caruthers, J.W. Fundamentals of Marine Acoustics. Amsterdam, Elsevier, 1977 [ISBN 0-444-41552-5]
- Clay, C.S. and Medwin, H. Acoustical Oceanography, Principles and Applications. New York, NY, Wiley, 1977 [ISBN 0-471-16041-5]
- Hamilton, E.L. Geoacoustic modeling of the ocean floor. *Journal of the Acoustical Society of America*, **68**, 1980: 1313–1340
- Jackson, D.R. and Briggs, K. B. High-frequency bottom backscattering: roughness versus sediment volume scattering. *Journal of the Acoustical Society of America*, **92**, 1992: 962–977.
- Jackson, D.R. Winebrenner, D.P. and Ishimaru, A., Application of the composite roughness model to high-frequency bottom backscattering. *Journal of the Acoustical Society of America*, **79**, 1986: 1410–1422
- Jensen, F.B., Kuperman, W.A., Porter, M.B. and Schmidt, H. Computational Ocean Acoustics. New York, NY, American Institute of Physics, 1994 [ISBN 1-56396-209-8]
- Kuo, E.Y.T. Wave scattering and transmission at irregular surfaces. *Journal of the Acoustical Society of America*, **36**, 1964: 2135–2142
- Lyons, A.P, Anderson, A.L. and Dwan, F.S. Acoustic scattering from the seafloor: Modeling and data comparison. *Journal of the Acoustical Society of America*, **95**, 1994: 2441–2451
- McKinney, C.M. and Anderson, C.D. Measurements of backscattering of sound from the ocean bottom. *Journal of the Acoustical Society of America*, **36**, 1964: 158–163
- Miles, J.W. On nonspecular reflection at a rough surface. *Journal of the Acoustical Society of America*, **26**, 1954: 191–199
- Mourad, P.D. and Jackson, D.R. A model/data comparison for low-frequency bottom backscatter. *Journal of the Acoustical Society of America*, **94**, 1993: 344–358
- Pierce, A.D., Acoustics: An Introduction to its Physical Principles and Applications, New York, NY, McGraw-Hill, 1981 [ISBN 0-07-049961-6]

Document Data Sheet

Security Classification		Project No.
		25
Document Serial No.	Date of Issue	Total Pages
SR-235	October 1995	50 pp.
Author(s)		
P.H. Rogers		
Title		
Detection of buried mines using Rayleigh-scattered second-derivative Gaussian pulses		
Abstract		
<p>Large ground mines which are intentionally or unintentionally buried in the sediment have proven to be difficult to detect. This report is the result of a study undertaken by the author while on leave from Georgia Tech at the NATO SACLANT Undersea Research Centre. It considers the possibility that low-frequency (200–500 Hz) pulses could be used to detect and localize buried mines. It has been shown that it may be possible to detect buried mines using Rayleigh scattered second derivative Gaussian pulses. The robustness of the method stems from the differences in mechanical properties of the mine and the wide range of bulk modulus and density of seafloor sediments.</p>		
Keywords		
buried mines, detection, Gaussian pulse, low frequency, Rayleigh scattering		
Issuing Organization		
North Atlantic Treaty Organization SACLANT Undersea Research Centre Viale San Bartolomeo 400, 19138 La Spezia, Italy [From N. America: SACLANTCEN CMR-426 (New York) APO AE 09613]		tel: +39-187-540.111 fax: +39-187-524.600 e-mail: library@saclantc.nato.int

Initial Distribution for SR-235

<u>Ministries of Defence</u>			
DND Canada	10	SCNR Norway	1
CHOD Denmark	8	SCNR Portugal	1
DGA France	8	SCNR Spain	1
MOD Germany	15	SCNR Turkey	1
HNDGS Greece	11	SCNR UK	1
MARISTAT Italy	10	SCNR US	2
MOD (Navy) Netherlands	12	French Delegate	1
NDRE Norway	10	SECGEN Rep. SCNR	1
MDN Portugal	5	NAMILCOM Rep. SCNR	1
MOD Spain	2		
TDKK Turkey	5	<u>National Liaison Officers</u>	
MOD UK	20	NLO Belgium	1
ONR US	54	NLO Canada	1
		NLO Denmark	1
		NLO Germany	1
<u>NATO Authorities</u>		NLO Italy	1
NAMILCOM	2	NLO Netherlands	1
		NLO UK	1
<u>SCNR for SACLANTCEN</u>		NLO US	1
SCNR Belgium	1		
SCNR Canada	1		
SCNR Denmark	1		
SCNR Germany	1		
SCNR Greece	1	Total external distribution	197
SCNR Italy	1	SACLANTCEN Library	23
SCNR Netherlands	1	Total number of copies	220